A giant comet-like cloud of hydrogen escaping the warm Neptune-mass exoplanet GJ 436b

David Ehrenreich[1], Vincent Bourrier[1], Peter J. Wheatley[2], Alain Lecavelier des Etangs[3,4], Guillaume Hébrard[3,4,5], Stéphane Udry[1], Xavier Bonfils[6,7], Xavier Delfosse[6,7], Jean-Michel Désert[8], David K. Sing[9], & Alfred Vidal-Madjar[3,4]

[1]Observatoire de l'Université de Genève, 51 chemin des Maillettes, 1290 Versoix, Switzerland

[2]Department of Physics, University of Warwick, Coventry CV4 7AL, UK

[3]CNRS, UMR 7095, Institut d'Astrophysique de Paris, 98bis boulevard Arago, 75014 Paris, France

[4]UPMC Univ. Paris 6, UMR 7095, Institut d'Astrophysique de Paris, 98 bis boulevard Arago, 75014 Paris, France

[5]Observatoire de Haute-Provence, CNRS & OAMP, 04870 Saint-Michel-l'Observatoire, France

[6]Univ. Grenoble Alpes, IPAG, F-38000 Grenoble, France

[7]CNRS, IPAG, F-38000 Grenoble, France

[8]CASA, Department of Astrophysical & Planetary Sciences, University of Colorado, 389-UCB, Boulder, CO 80309, USA

[9]Astrophysics Group, School of Physics, University of Exeter, Stocker Road, Exeter EX4 4QL

Exoplanets orbiting close their parent stars could lose some fraction of their atmospheres because of the extreme irradiation[1-5]. In particular, it has been suggested that large and hot rocky planets[6] might have lost all of their atmosphere, having begun as Neptune-like[7-12]. It has been predicted that the signature of this loss would be visible in the ultraviolet[13], with transits extended in depth and duration beyond those visible in the optical. Here we report that in the ultraviolet the Neptune-mass exoplanet GJ 436b has transits eclipsing 56.3±3.5% of the stellar surface, far beyond the 0.69% occultations caused by the optical transits. The ultraviolet transits start ~2 hrs before, and end >3 hrs after the optical transits, which last for ~1 hr. We infer from this that the planet is surrounded and trailed by a large exospheric cloud composed mainly of hydrogen atoms on ballistic trajectories. Although atmospheric mass loss primarily affects low-mass exoplanets, no confident measurements were previously available. The unambiguous detection (16.0σ) at GJ 436b allows an estimation for the mass-loss rate in the range of ~10^8–10^9g s^{-1}, which today is far too small to deplete the atmosphere of a Neptune-like planet in the lifetime of the parent star, but would have been much greater in the past. These observations opens the exciting possibility that large atmospheric signals could be retrieved in the UV for a whole population of moderately irradiated, low-mass exoplanets.

Three transits of GJ 436b, which occur every 2.64 days, have been observed on 7 December 2012[4] (visit 1), 18 June 2013 (visit 2), and 23 June 2014 (visit 3) with the Space Telescope Imaging Spectrograph (STIS) on board the Hubble Space Telescope (HST). A stellar spectrum acquired using similar settings in January 2010[13] (visit 0) was retrieved from the archive for comparison purposes. HST data in visits 2 and 3 were complemented with simultaneous Chandra X-ray observations. The HST data consist of time-tagged, far-ultraviolet spectra obtained with a grating dispersing light over the 1,195–1,248 Å domain, with a spectral resolution of ~20 km s^{-1} at 1,215.6 Å (the Lyman-α transition of atomic hydrogen, H I). Exposure times of 1,800 s to 2,400 s were used to observe the star for four successive HST orbits during each visit. Each HST orbit lasts for 96 min, during which GJ 436 is visible for 56 min before being occulted by the Earth, yielding 40 min gaps in the data.

The most prominent spectral feature is the H I Lyman-α emission (Figure 1) arising in M dwarf stars from the transition region between the chromosphere and the corona. Absorption in this line has been reported in other systems, during transits of hot Jupiters. This is interpreted by the presence of escaping hydrogen exospheres surrounding close-in gas giants[1,3,14]. If GJ 436b possesses such an extended atmosphere, we should thus observe a time-resolved absorption signature over the stellar Lyman-α emission. A tentative detection was made from visit 1 data despite the signal being observed only after the optical transit of the planet[4]. Visits 2 and 3 have been specifically carried out to search for a signal related to the optical transit.

We performed a careful analysis to check for the existence of instrumental systematics in the data and correct for them (see the Supplementary Information). Large variations are detected over a localised part of the stellar Lyman-α line at times corresponding to the optical transit, which cannot be explained by any known instrumental effects. The most significant absorption occurs in the blue wing of the line for radial velocities between –120 km s^{-1} to –40 km s^{-1}, during the three visits. In this interval, shown in Figure 1, the Lyman-α line is absorbed with respect to the reference spectrum ("out-of-transit phases") about 2 hrs before the optical transit mid-time ("pre-transit phases"). Averaged over the three visits, which all show remarkably similar behaviour (see Extended Data Figure 1), the pre-transit stellar flux in the blue wing of the line is absorbed by 17.6±5.2% with respect to the out-of-transit flux. The absorption keeps increasing around the mid-transit time ("in-transit phases"), where the stellar flux is absorbed by 56.2±3.6%. At this time, an equivalent surface larger than half the stellar disc is eclipsed. After the end of the optical transit ("post-transit phases"), the absorption signal at Lyman-α slightly decreases to 47.2±4.1%. This transit signature, plotted in Figure 2, is significantly deeper than the one of 22.9±3.9% previously reported for visit 1 data alone[4] and starts significantly earlier (~2.7 hrs); the difference is mainly due to our finding of a pre-transit absorption and updated transit ephemeris (see the Supplementary Information).

In sharp contrast with the huge signature observed between –120 km s^{-1} and –40 km s^{-1}, the flux remains stable at larger blue shifts, and over the whole red-shifted wing of the line, as shown in Figure 2. In the red wing of the line (between +20 km s^{-1} and +200 km s^{-1}), flux ratios of 0.7±3.6%, 1.7±3.5%, and 8.0±3.1% are measured during the pre-transit, in-transit, and post-transit phases, respectively, which is compatible with no detection at the 3σ level.

Absorption signals shallower and shorter than for GJ 436b have been reported during transits of hot Jupiters, in the blue wing of their host star Lyman-α lines[1,3,14,15]. These signals are all interpreted as absorption by extended upper atmospheres around the planets. Meanwhile, magnetic activity could also induce variations in the stellar emission. We use the unabsorbed red part of the line to estimate that the intrinsic stellar variability at GJ 436 should not exceed 5% to 11% of the Lyman-α flux during one visit. Our Chandra X-ray data cover pre-transit phases at four epochs (see the Supplementary Information), two of which during HST visits 2 and 3. They show very similar extreme UV (EUV) emission, supporting small stellar variability between HST visits at Lyman-α. We conclude that stellar variability cannot explain the observed decrease at Lyman-α, at times coinciding with the planetary transits.

We propose that the asymmetric absorption is caused by the passage of a huge hydrogen cloud, surrounding and trailing the planet. The planetary atmosphere is an obvious source for this hydrogen. We test this assumption by showing that the observed Lyman-α light curve can be reproduced with a simple transiting shape. We use an optically-thick ellipse of semi-major axis a and semi-minor axis b to represent the projection of the cloud in the plan of the sky. We calculate the transit light curve that such a cloud would produce when passing in front of the star, as seen from Earth, and fit it to the light curve, adjusting for a and b. A best fit is obtained for $a = 12.1\ R_*$ and $b = 2.4\ R_*$ and the corresponding light curve and cloud contour are plotted in Figure 2 (thick grey curve) and Figure 3, respectively. The cloud extends far beyond the planet Roche lobe radius (4.42 R_p or 0.37 R_*), a spatial extension unmatched by any of the observations of hot Jupiters. The transit of GJ 436b is grazing so we assume the cloud would transit with a similar inclination, corresponding to an impact parameter of 0.8521[16]. Remarkably, a central transit would have totally eclipsed the star and we surmise that this should happen in the case of other red dwarfs exhibiting central transits from planets similar to GJ 436b. Future ultraviolet observations of systems similar to GJ 436 could potentially reveal total Lyman-α eclipses.

The fact that the absorption signal takes place in the [–120,–40] km s^{-1} interval yields additional constraints on the dynamics of the hydrogen atoms and the 3D structure of the exospheric cloud. First, the whole velocity range is in excess of the planet escape velocity (~26 km s^{-1} at the planet surface), consistent with gas escaping from the planet. The acceleration mechanism of hydrogen atoms escaping from highly-irradiated hot Jupiters is debated: after hydrogen atoms escape the planets with initial velocities dominated by the orbital velocity (~100 km s^{-1} for GJ 436b in the host star reference frame), they are submitted to the stellar radiation pressure, can interact with the stellar wind, and are eventually ionised by stellar extreme UV (EUV; 10–91.2 nm) radiation. Radiation pressure is measurable from resolved observation of the Lyman-α profile, which has to be corrected for the interstellar medium absorption[13,17]. For strong lines such as Lyman-α, radiation pressure can overcome the stellar gravitation, repelling the escaping atoms towards the observer, and producing a blue-shifted signature. In one hot Jupiter (HD 189733b), the absorption observed at very large blue-shift is best explained by charge exchange interaction with the stellar wind, creating energetic neutral atoms (ENAs) with large negative (blue-shifted) radial velocities[15,18-20]. In other cases[1,14,21], radiation pressure alone explain the observed radial velocities of the escaping gas.

We run our 3D numerical simulation of atmospheric escape[15] to understand the origin of the absorption signature in radial velocity observed in the blue wing of the stellar Lyman-α line. The line profile corrected from interstellar absorption is used to calculate the stellar radiation pressure on hydrogen atoms. These are released isotropically from the Roche lobe limit of GJ 436b, with velocities dominated by the tangential orbital velocity of the planet at the time of their release. The calculation takes the orbital eccentricity of GJ 436b ($e = 0.15$) into account. The main parameters of the atmospheric escape model are the mass-loss rate $\dot{m}$ of hydrogen lost by the planet and the photo-ionisation rate α_{EUV} of hydrogen atoms. The model computes the structure of the escaping gas cloud as well as its radial velocity absorption signature. A family of models, with parameters in the ranges of $\dot{m} \sim 10^8$–10^9 g s^{-1} and $\alpha_{\mathrm{EUV}} \sim 8\times10^{-7}$–$3\times10^{-6}$ s^{-1} (implying neutral atom lifetimes of ~4–18 min at the distance of the planet), provides good fits to the data; an example light curve is plotted in Figure 2. The model correctly predicts the ~2 hr early UV transit ingress observed with respect to the optical transit, as well as the transit depth in the correct range of velocities. It provides a good match to the re-analysed visit 1 data. It furthermore predicts that the UV transit could last up to ~20 hrs after the optical transit, due to the extended hydrogen tail of the exospheric cloud. More UV observations will be needed to verify this prediction.

According to the numerical simulation, the stellar radiation pressure counterbalances $\lesssim$70% of the star's gravity pull on the escaping atoms, which is much less than in other systems with hot Jupiters, where radiation pressure takes over stellar gravity by factors of 3 to 5[15]. The low stellar radiation pressure at GJ 436b allows the formation of a large coma and tail of escaping atoms, comoving with the planet although not gravitationally bounded to it.

Atmospheric escape is involved in the possible loss of a whole population of irradiated exoplanets[8,9,11,12]. The average mass-loss rate of $\sim 5\times10^{8}$ g s^{-1} at GJ 436b means that the planet loses ~0.1% of its atmosphere per billion years (assuming it accounts for 10% of the planet mass, like Neptune). This rate requires ~1% efficiency in the conversion of input energy into mass loss[11]. In the past, an M dwarf like GJ 436 was more active and the planet could have received $\lesssim$100 times more X-ray and EUV irradiation over ~1 Gyr[22], resulting in a possible loss of $\lesssim$10% of its atmosphere during the first billion years. This planet thus stands on the edge of significant mass loss, leading us to surmise that closer-in Neptunes could have evolved more dramatically because of atmospheric escape.

This 16.0σ detection opens the exciting perspective to obtain large atmospheric signals from comet-like exospheres around moderately-irradiated, low-mass planets in the UV, while the atmospheric characterisation of similar planets remains challenging at longer wavelengths[23]. Over ~10,000 nearby systems like GJ 436 will be discovered by upcoming transit surveys carried out from the ground (e.g. NGTS) and from space (K2, CHEOPS, TESS, and PLATO).

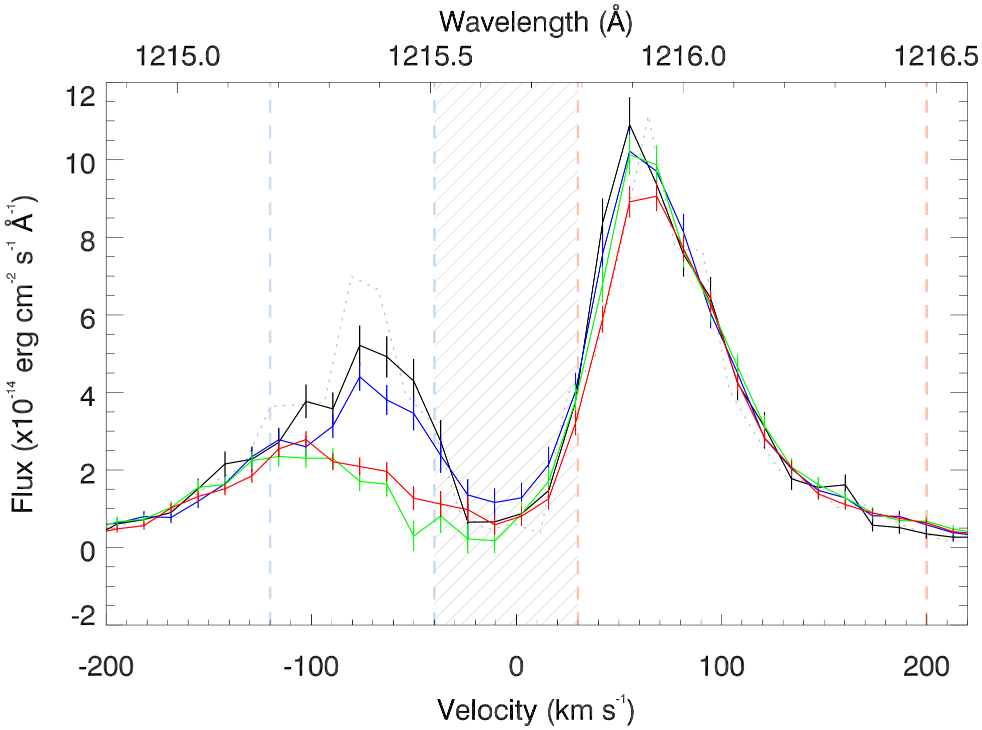

Figure 1 | Spectra of the star GJ 436 taken with the Space Telescope Imaging Spectrograph of the Hubble Space Telescope. The region around the Lyman-α emission of atomic hydrogen (H I) is shown in heliocentric velocity space, with 0 km s^{-1} corresponding to a wavelength of 121.56 nm. The line core (grey hatched region) cannot be observed from Earth because of absorption by hydrogen in the interstellar medium (ISM) along the line of sight. The ISM absorption produces this characteristic double-peak profile. The different colours show the stellar emission averaged over all HST visits at different phases with respect to the optical transit: out-of-transit (black), pre-transit (blue), in-transit (green), and post-transit (red). The absorption signal is measured in the blue-shifted part of the line (corresponding to negative radial velocities) in the range of [–120,–40] km s^{-1}, delimited by the vertical blue dashed lines. A control measure is performed over the red-shifted part of the line in the range of [+30,+200] km s^{-1} delimited by the vertical red dashed lines. The stellar line profile observed in January 2010 (visit 0) is shown for comparison with a dotted grey line.

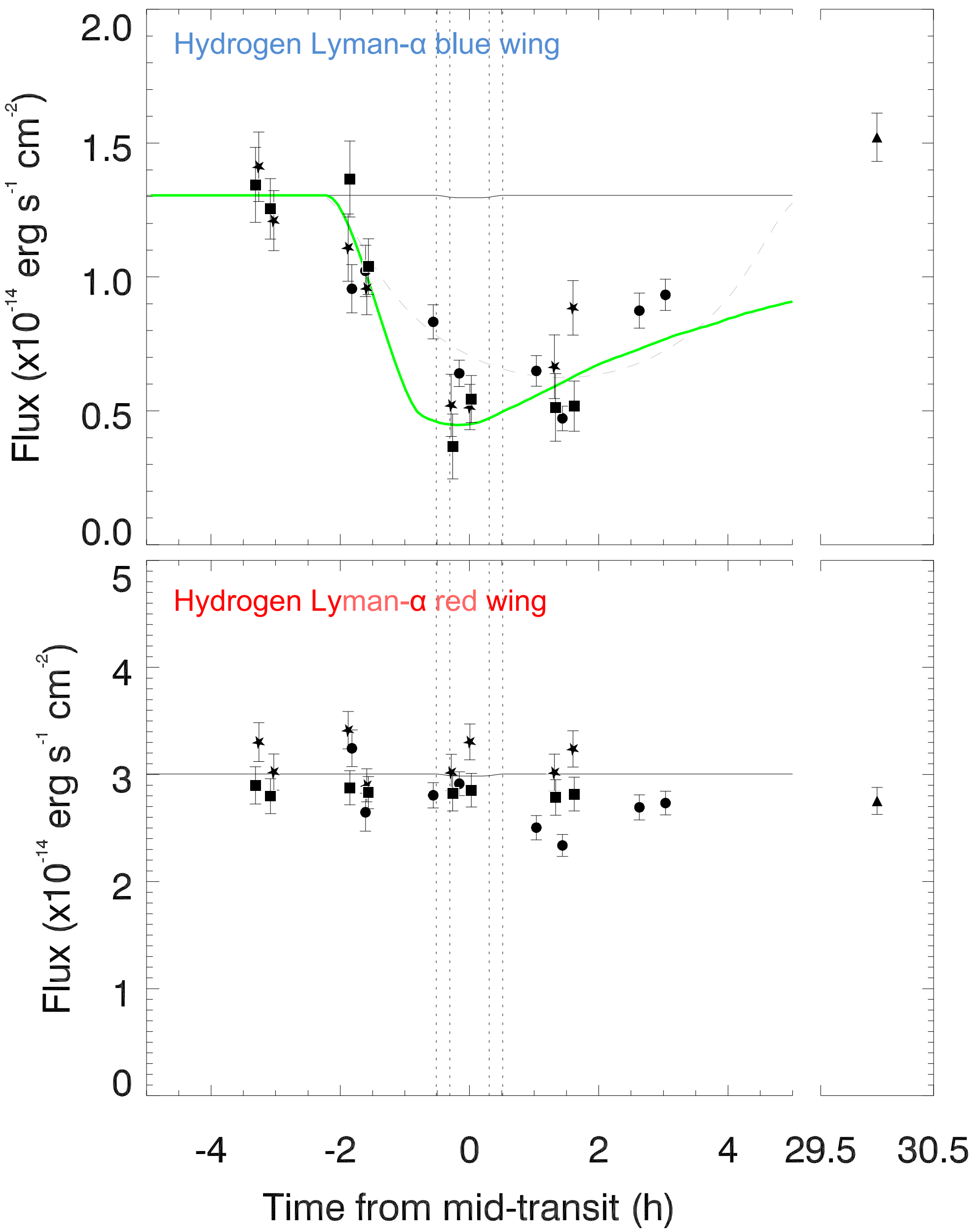

Figure 2 | Ultraviolet transit light curves of GJ 436b. They are calculated by integrating the stellar hydrogen Lyman-α line in the velocity ranges [–120,–40] km s^{-1} (blue wing of the line; top panel) and [+30,+200] km s^{-1} (red wing of the line; bottom panel). The different observation epochs are represented with different symbols for visit 1 (circles), visit 2 (stars), visit 3 (squares), and visit 0 (triangle). The data point from visit 0[13], acquired ~3 years before visit 1, shows that the out-of-transit variability is small compared to the blue-shifted signal observed in the in-transit and post-transit phases. The planetary transit observed in the optical is shown to scale by the thin black line: with an absorption depth of 0.69%, it is barely seen at this scale. The vertical dotted line represent the contact points of this transit. The ultraviolet transit in the blue wing of the line is far deeper and wider than the shallow optical transit, starting about 2 hrs before the mid-transit time and lasting for at least 3 hrs after it. No such behaviour is observed in the red wing of the line. The decrease of the red-wing flux during the post-transit phases has been noticed by ref.[[4]] for the visit 1 data. This behaviour is, however, not reproduced during visits 2 and 3, and the mean post-transit absorption of 8.0±3.1% in the red wing has a significance of 2.6σ only. The grey dashed curve in the top panel is the best-fit transit light curve of the optically thick ellipsoidal model. The contour of this ellipse is represented in Figure 3. The thick green curve show one of the best-fit transit light curve generated with the 3D particle simulation[15].

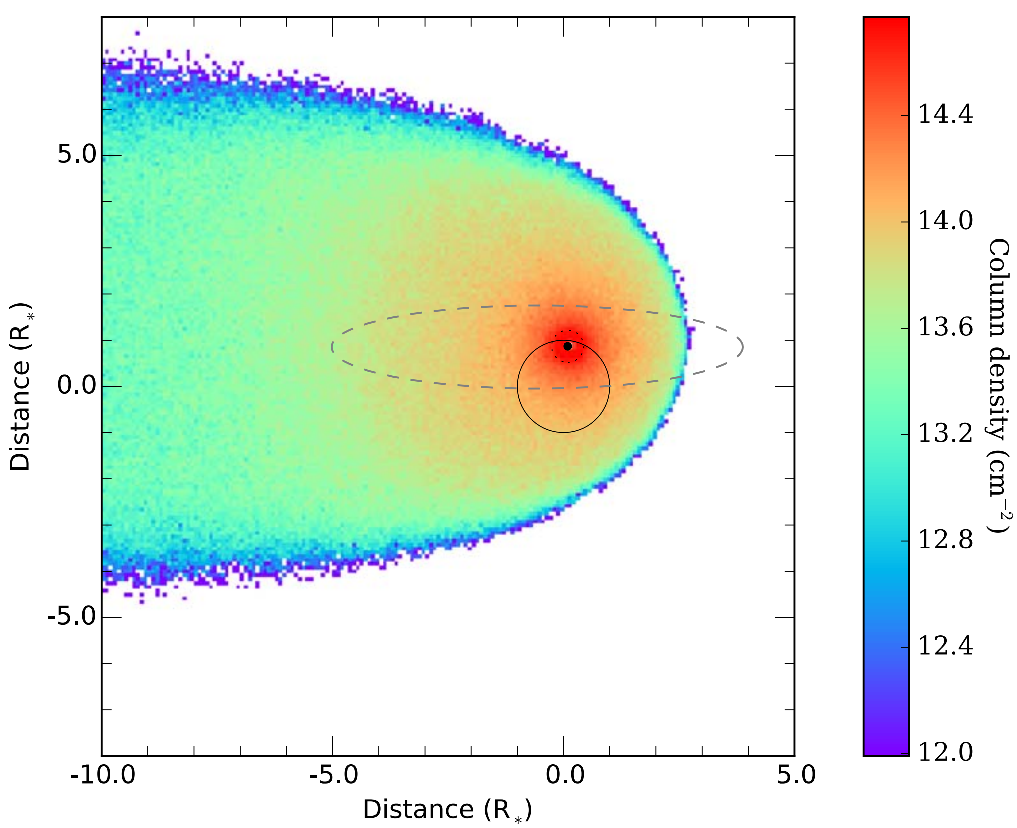

Figure 3 | Particle simulation[15] showing an optically-thin comet-like exospheric cloud transiting the star (large white circle), as seen from Earth. GJ 436b is the small black dot represented at mid-transit at 0.8521 stellar radius[16] from the centre of the star, which is figured by the black circle. The dotted circle around the planet represents its equivalent Roche radius The colour of simulation particles denotes the column density of the cloud. The transit of this simulated cloud gives rise to absorption over the blue wing of the Lyman-α line represented by the green light curve in the top panel of Figure 2. The dashed grey ellipse delimits the best-fit optically-thick cloud from the geometrical toy model, which produces the dashed grey light curve in the top panel of Figure 2.

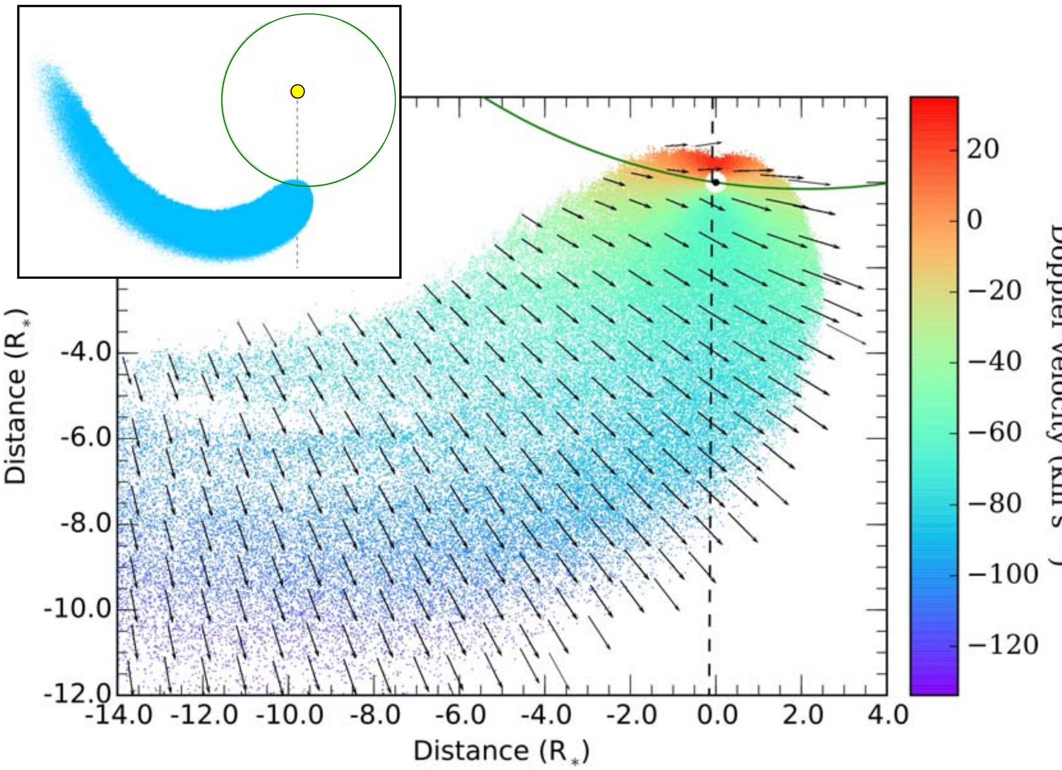

Figure 4 | Image of 3D simulation representing a slice of the comet-like cloud coplanar with the line of sight (dashed vertical line), as viewed from "above". The arrows represent the hydrogen atom velocity and direction in the rest frame of the star. Particles are colour-coded as a function of their projected velocities on the line of sight (the dashed vertical line). The inset shows a zoom out of this image to the full spatial extent of the exospheric cloud (in blue). The planet orbit is shown to scale with the green ellipse and the star is represented with the yellow circle.

References

1. Vidal-Madjar, A. et al. An extended upper atmosphere around the extrasolar planet HD209458b. Nature 422, 143 (2003).
2. Fossati, L. et al. Metals in the Exosphere of the Highly Irradiated Planet WASP-12b. The Astrophysical Journal Letters 714, L222 (2010).
3. Lecavelier des Etangs, A. et al. Temporal variations in the evaporating atmosphere of the exoplanet HD 189733b. Astronomy and Astrophysics 543, L4 (2012).
4. Kulow, J. R., France, K., Linsky, J. & Loyd, R. O. P. Lyα Transit Spectroscopy and the Neutral Hydrogen Tail of the Hot Neptune GJ 436b. ApJ 786, 132 (2014).
5. Koskinen, T. T., Aylward, A. D. & Miller, S. A stability limit for the atmospheres of giant extrasolar planets. Nature 450, 845–848 (2007).
6. Pepe, F. et al. An Earth-sized planet with an Earth-like density. Nature 503, 377–380 (2013).
7. Lecavelier des Etangs, A., Vidal-Madjar, A., McConnell, J. C. & Hébrard, G. Atmospheric escape from hot Jupiters. Astronomy and Astrophysics 418, L1–L4 (2004).
8. Lecavelier des Etangs, A. A diagram to determine the evaporation status of extrasolar planets. Astronomy and Astrophysics 461, 1185–1193 (2007).
9. Davis, T. A. & Wheatley, P. J. Evidence for a lost population of close-in exoplanets. Monthly Notices RAS 396, 1012 (2009).
10. Jackson, B. et al. The roles of tidal evolution and evaporative mass loss in the origin of CoRoT-7 b. Monthly Notices RAS 407, 910–922 (2010).
11. Ehrenreich, D. & Désert, J.-M. Mass-loss rates for transiting exoplanets. Astronomy and Astrophysics 529, 136 (2011).
12. Lopez, E. D., Fortney, J. J. & Miller, N. How Thermal Evolution and Mass-loss Sculpt Populations of Super-Earths and Sub-Neptunes: Application to the Kepler-11 System and Beyond. ApJ 761, 59 (2012).
13. Ehrenreich, D., Lecavelier des Etangs, A. & Delfosse, X. HST/STIS Lyman-α observations of the quiet M dwarf GJ 436. Predictions for the exospheric transit signature of the hot Neptune GJ 436b. Astronomy and Astrophysics 529, 80 (2011).
14. Ehrenreich, D. et al. Hint of a transiting extended atmosphere on 55 Cancri b. Astronomy and Astrophysics 547, 18 (2012).
15. Bourrier, V. & Lecavelier des Etangs, A. 3D model of hydrogen atmospheric escape from HD 209458b and HD 189733b: radiative blow-out and stellar wind interactions. Astronomy and Astrophysics 557, 124 (2013).
16. Knutson, H. A. et al. A Spitzer Transmission Spectrum for the Exoplanet GJ 436b, Evidence for Stellar Variability, and Constraints on Dayside Flux Variations. ApJ 735, 27 (2011).
17. France, K. et al. The Ultraviolet Radiation Environment around M dwarf Exoplanet Host Stars. ApJ 763, 149 (2013).
18. Holmström, M. et al. Energetic neutral atoms as the explanation for the high-velocity hydrogen around HD 209458b. Nature 451, 970 (2008).
19. Ekenbäck, A. et al. Energetic Neutral Atoms Around HD 209458b: Estimations of Magnetospheric Properties. ApJ 709, 670 (2010).
20. Bourrier, V. et al. Atmospheric escape from HD 189733b observed in H I Lyman-α: detailed analysis of HST/STIS September 2011 observations. Astronomy and Astrophysics 551, 63 (2013).
21. Bourrier, V., Lecavelier des Etangs, A. & Vidal-Madjar, A. Modeling magnesium

escape from HD 209458b atmosphere. Astronomy and Astrophysics 565, 105 (2014).
22. Ribas, I., Guinan, E. F., Güdel, M. & Audard, M. Evolution of the Solar Activity over Time and Effects on Planetary Atmospheres. I. High-Energy Irradiances (1-1700 Å). ApJ 622, 680 (2005).
23. Knutson, H. A., Benneke, B., Deming, D. & Homeier, D. A featureless transmission spectrum for the Neptune-mass exoplanet GJ[thinsp]436b. Nature 505, 66–68 (2014).
24. Poppenhaeger, K., Robrade, J. & Schmitt, J. H. M. M. Coronal properties of planet-bearing stars. Astronomy and Astrophysics 515, 98 (2010).
25. Sanz-Forcada, J. et al. Estimation of the XUV radiation onto close planets and their evaporation. Astronomy and Astrophysics 532, A6 (2011).
26. Pont, F., Gilliland, R. L., Knutson, H., Holman, M. & Charbonneau, D. Transit infrared spectroscopy of the hot Neptune around GJ 436 with the Hubble Space Telescope. Monthly Notices RAS Letters 393, L6 (2009).
27. Chadney, J. M., Galand, M., Unruh, Y. C., Koskinen, T. T. & Sanz-Forcada, J. XUV-driven mass loss from extrasolar giant planets orbiting active stars. ICARUS 250, 357–367 (2015).
28. Linsky, J. L., Fontenla, J. & France, K. The Intrinsic Extreme Ultraviolet Fluxes of F5 V TO M5 V Stars. ApJ 780, 61 (2014).
29. Lanotte, A. A. et al. A global analysis of Spitzer and new HARPS data confirms the loneliness and metal-richness of GJ 436 b. Astronomy and Astrophysics 572, A73 (2014).

Supplementary Information is linked to the online version of the paper at www.nature.com/nature.

Acknowledgements This work bas been carried out in the frame of the National Centre for Competence in Research 'PlanetS' supported by the Swiss National Science Foundation (SNSF). D.E., V.B., and S.U. acknowledge the financial support of the SNSF.

Author Contributions D.E. proposed and led the HST-Chandra joint observation programme, supervised data reduction and analysis, interpreted the results, and wrote the paper. V.B. performed data reduction and analysis, and computer simulations to interpret the results. P.J.W. set the Chandra X-ray observations, reduced, analysed, and interpreted the X-ray data. A.L. co-designed the simulation programme with V.B. and provided computing resources to run the simulations. A.L. and G.H. contributed to the observation programme, data analysis, and interpretation. S.U., X.B., X.D., J.-M.D., D.K.S., and A.V.-M. contributed to the observation programme and interpretation. All authors discussed the results and commented on the manuscript.

Author Information Reprints and permissions information is available at www.nature.com/reprints. Correspondence and requests for materials should be addressed to D.E. (david.ehrenreich@unige.ch).